EUROPEAN COOPERATION
IN SCIENCE
AND TECHNOLOGY

EURO-COST

CA15104TD(21)14023
Online Meeting
February 8 - 9, 2021

SOURCE: ULB, Université Libre de Bruxelles, Belgium
UCL, Université catholique de Louvain, Belgium
IBGE, Bruxelles Environnement, Belgium
Télécom Paris – LTI, France

A stochastic geometry approach to EMF exposure modeling

Quentin Gontier, Luca Petrillo, François Rottenberg, François Horlin, Joe Wiart, Claude Oestges,

Philippe De Doncker

Quentin Gontier
ULB, Université Libre de Bruxelles
Avenue Franklin Roosevelt 50 165/81
1050 Bruxelles,
BELGIUM
Email: quentin.gontier@ulb.be

A stochastic geometry approach to EMF exposure modeling

QUENTIN GONTIER[1*], LUCA PETRILLO[2], FRANÇOIS ROTTENBERG[1, 4], FRANÇOIS HORLIN[1], JOE WIART[3], CLAUDE OESTGES[4], AND PHILIPPE DE DONCKER[1]

[1] *Wireless Communications Group Department, Université libre de Bruxelles, Belgium*
[2] *Bruxelles Environnement (IBGE) - Leefmilieu Brussel (BIM), Belgium*
[3] *Télécom Paris - LTI, C2M Chair, Palaiseau, France*
[4] *ICTeam Department, UCLouvain, Belgium*
[*] *Corresponding author: quentin.gontier@ulb.be*
[/] *This work was supported in part by the FNRS under MUSE-WINET EOS grant and Innoviris under STOEMP-EMF grant.*

Compiled February 3, 2021

Downlink exposure to electromagnetic fields (EMF) in urban environments is studied using the stochastic geometry (SG) framework. A 2D Poisson point process (PPP) is assumed for the base station (BS) distribution and the height of the base stations is taken into account in the propagation model. From simple assumptions, mathematical expressions of statistics of exposure are derived from the model. The error made by taking a reduced number of base stations, instead of the whole set of base stations, is quantified. A sensitivity analysis is proposed in order to evaluate the impact of the model parameters on the statistics of exposure. The method is then applied to two Brussels municipalities, in Belgium, for the UMTS 2100 and LTE 2600 frequency bands. It is shown that the proposed model fits experimental values, paving the way to a new methodology to assess general public exposure to electromagnetic fields.

cellular networks, exposure, Poisson point process, stochastic geometry

1. INTRODUCTION

Electromagnetic field (EMF) exposure due to cellular networks is classically evaluated either through in-situ measurements [1], drive-tests or sensor networks [2] [3], or by using ray-tracing softwares [4]. Numerically, this evaluation is however difficult to obtain deterministically in a reasonable time. It is also subject to many uncertainties (due to the number of base stations in operation, the environment geometry, the presence of people and vehicles causing shadowing...). A deterministic computation of EMF exposure at every point of the area under study is not always required. Instead, statistical values are often looked for, for instance to estimate the probability of exceeding some exposure thresholds, or to estimate the mean level of exposure. This paper aims to lay the foundations of a statistical study of exposure to electromagnetic fields due to cellular networks, using stochastic geometry (SG) and a simple parametric propagation model.

Using SG in wireless communications is now an old concept [5]. It has been applied in many fields, ranging from automotive radar [6], to localization [7], including probability of coverage and spectral efficiency [8], cumulated interference power [9] and outage probability [10] but to our knowledge, only one recent article exploits it for exposure assessment [11].

EMF exposure is usually written in terms of incident EMF power density S ($\mathrm{W/m^2}$) [12] [13]. Power density may then be translated into electric field strength ($\mathrm{V/m}$) to define exposure limits:

$$E = \sqrt{Z_0\, S} \tag{E1}$$

where $Z_0 = \sqrt{\mu_0/\epsilon_0} = 120\pi \approx 377\Omega$ is the impedance of free-space.

In the first part of this paper, mathematical expressions are derived to evaluate the statistics and cumulative distribution function (CDF) of the power density emitted by

a random pattern of cellular BSs. In the second part, we fit and validate the model using experimental data obtained in two municipalities of the Brussels-Capital Region, in Belgium in the UMTS 2100 and the LTE 2600 frequency bands.

2. SG MODEL OF EXPOSURE

A. Exposure model

In the SG approach, the BS spatial distribution is considered as a random point pattern with constant density λ in a given 2D region $\mathcal{W}$, referred to as the *window*. According to [14] considering together the BSs of all network providers, BS patterns in European cities are well modeled using homogeneous 2D-Poisson Point Processes $\Phi \in \mathbb{R}^2$ (PPP): for any $\mathcal{W}$, the number of points falling in $\mathcal{W}$ has a Poisson distribution with mean $\lambda \cdot \tau_2(\mathcal{W})$,where $\tau_2(\mathcal{W})$ is the area of $\mathcal{W}$. It implies that measures do not depend on the location in space where the computation is performed.

For any BS of the PPP, the received power density S can be deduced from a path loss model

$$S(r) = \frac{A}{\left(r^2 + h^2\right)^{\alpha/2}}, \tag{E2}$$

where $S(r)$ is the power density due to the BS located at horizontal distance r, h the height of the BS, α is the path loss exponent (typically ranging from 2 to 5) and A a multiplicative random variable modeling channel fading and the effective isotropic radiated powers (EIRP) of the BS. A can be written $A = p \cdot B$ with $p = \frac{\text{EIRP}}{4\pi}$ and B is any random variable modeling fading. It is worth noting that, in our approach, the BS network is homogenized in the sense that BSs share common features in terms of height and EIRP.

For all BSs of all network providers present in the PPP, the power densities can be summed up, assuming that all signals are uncorrelated, to get S_{WN}, the total EMF power density and hence the total exposure for the whole network of BSs (WN)

$$S_{WN} = \sum_{i|BS_i \in \Phi} S(r_i) = \sum_{i|BS_i \in \Phi} \frac{A}{\left(h^2 + r_i^2\right)^{\alpha/2}}. \tag{E3}$$

B. Exposure due to the n^{th}th nearest BS

We start by studying separately the contribution of each BS of the PPP. Let $S_n = S_n(r)$ be the power density due to the n^{th} nearest BS to the calculation point. The probability density function (PDF) of the distance to the n^{th} nearest BS is given by the Erlang distribution of order n [15]

$$f(r_n) = 2\frac{(\lambda\pi)^n}{(n-1)!} r_n^{2n-1} \mathrm{e}^{-\lambda\pi r_n^2}. \tag{E4}$$

Using this PDF with $n = 1$, the mean value of the power density due to the nearest BS can be obtained as

$$\begin{aligned}
\mathbb{E}[S_1] &= \mathbb{E}\left[\frac{A}{\left(r_1^2 + h^2\right)^{\alpha/2}}\right] \\
&= \overline{A} \cdot \mathbb{E}\left[\frac{1}{\left(r_1^2 + h^2\right)^{\alpha/2}}\right] \\
&= 2\pi\lambda\,\overline{A} \int_0^\infty \frac{1}{\left(r^2 + h^2\right)^{\alpha/2}} r\,\mathrm{e}^{-\lambda\pi r^2}\,\mathrm{d}r \\
&= (\lambda\pi)^{\alpha/2}\,\overline{A}\,\mathrm{e}^{\lambda\pi h^2}\,\Gamma\left(1 - \frac{\alpha}{2}, \lambda\pi h^2\right),
\end{aligned} \tag{E5}$$

with $\overline{A} = \mathbb{E}[A]$. The upper incomplete Gamma function $\Gamma(z,t)$ is defined as

$$\Gamma(z,t) = \int_t^\infty u^{z-1}\,\mathrm{e}^{-u}\,\mathrm{d}u, \qquad \Re(z) > 0. \tag{E6}$$

When $\alpha > 2$, the last expression of (E5) is not properly defined since the first argument of the incomplete Gamma function, $1 - \frac{\alpha}{2}$, is negative. In this case, the Gauss continued fraction can nonetheless be used for numerical calculations [16]:

$$\Gamma(z,t) = \cfrac{t^z \mathrm{e}^{-t}}{t + \cfrac{1-z}{1 + \cfrac{1}{t + \cfrac{2-z}{1 + \cfrac{2}{t + \cfrac{3-z}{1 + \ddots}}}}}} \tag{E7}$$

In the following, $\tilde{\Gamma}_i$ will be used as a simplified notation for $\Gamma\left(i, \lambda\pi h^2\right)$. The expected value for the n^{th} nearest BS was calculated using (E4):

$$\begin{aligned}
\mathbb{E}[S_n] &= \overline{A}\,\frac{2\,(\lambda\pi)^n}{(n-1)!} \int_0^\infty \frac{1}{\left(r^2 + h^2\right)^{\alpha/2}} r^{2(n-1)}\,\mathrm{e}^{-\lambda\pi r^2}\,r\,\mathrm{d}r \\
&\overset{(a)}{=} \overline{A}\,\frac{(\lambda\pi)^n\,(\lambda\pi)^{\alpha/2-1}}{(n-1)!}\,\mathrm{e}^{\lambda\pi h^2} \\
&\quad \times \int_{\lambda\pi h^2}^\infty t^{-\alpha/2}\,\mathrm{e}^{-t}\left(\frac{t}{\lambda\pi} - h^2\right)^{n-1}\mathrm{d}t \\
&\overset{(b)}{=} \overline{A}\,\frac{(\lambda\pi)^n\,(\lambda\pi)^{\alpha/2-1}}{(n-1)!}\,\mathrm{e}^{\lambda\pi h^2} \\
&\quad \times \int_{\lambda\pi h^2}^\infty t^{-\alpha/2}\,\mathrm{e}^{-t} \sum_{l=0}^{n-1} \binom{n-1}{l} \left(\frac{t}{\lambda\pi}\right)^l \left(-h^2\right)^{n-1-l}\mathrm{d}t \\
&= \overline{A}\,(\lambda\pi)^{\alpha/2}\,\mathrm{e}^{\lambda\pi h^2} \sum_{l=0}^{n-1} \frac{\left(-\lambda\pi h^2\right)^{n-l-1}}{l!\,(n-l-1)!}\,\tilde{\Gamma}_{1+l-\alpha/2},
\end{aligned} \tag{E8}$$

where we used (a) the change of variable $r^2 \to \frac{t}{\lambda\pi} - h^2$ and (b) the Binomial theorem. This result can also be written using $\mathbb{E}[S_1]$:

$$\mathbb{E}[S_n] = \mathbb{E}[S_1] \cdot \Xi_n^{[1]} \tag{E9}$$

where

$$\Xi_n^{[1]} = \sum_{l=1}^{n} \frac{\left(-\lambda\pi h^2\right)^{n-l}}{(l-1)!\,(n-l)!} \frac{\tilde{\Gamma}_{l-\alpha/2}}{\tilde{\Gamma}_{1-\alpha/2}}, \tag{E10}$$

using the change of index $l+1 \to l$. Fig. F1 shows the ratio (E10) as a function of n. As can be seen from this figure, for the set of parameters that will be identified in section 3, the nearest BS provides the main contribution to exposure but the second BS is also important since $\Xi_2^{[1]}/\Xi_1^{[1]} \approx 23\%$. From the fifth nearest BS, the contribution becomes negligible since $\Xi_{n|n>4}^{[1]}$ is less than 5%.

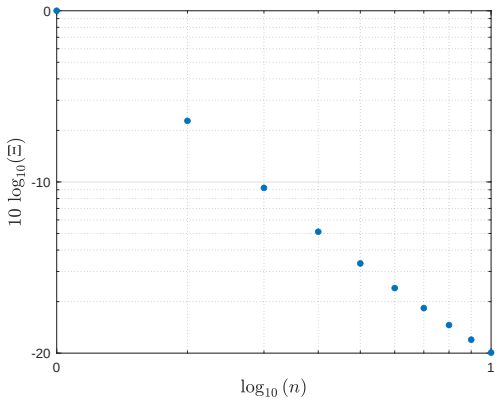

Fig. F1. Ratio between the mean value of the power density coming from the n^{th} nearest BS and the mean value of the power density coming from the nearest BS as a function of n. $\lambda = 13\,\text{BS/km}^2$, $\alpha = 2.90$, $h = 44\,\text{m}$, EIRP = 68.49 dBm.

Similarly, the k^{th} moment about zero for the field coming from the n^{th} BS is given by

$$\mathbb{E}\left[S_n^k\right] = \overline{A^k}\,(\lambda\pi)^{k\alpha/2}\,\mathrm{e}^{\lambda\pi h^2} \sum_{l=0}^{n-1} \frac{\left(-\lambda\pi h^2\right)^{n-l-1}}{l!\,(n-l-1)!}\,\tilde{\Gamma}_{1+l-k\alpha/2}, \tag{E11}$$

allowing to compute any moment of S_n. Again, this equation can make $\mathbb{E}\left[S_n^k\right]$ appear, generalizing $\Xi_n^{[k]}$ for the order k:

$$\mathbb{E}\left[S_n^k\right] = \mathbb{E}\left[S_1^k\right] \cdot \Xi_n^{[k]}, \tag{E12}$$

$$\Xi_n^{[k]} = \sum_{l=1}^{n} \frac{\left(-\lambda\pi h^2\right)^{n-l}}{(l-1)!\,(n-l)!} \frac{\tilde{\Gamma}_{l-k\alpha/2}}{\tilde{\Gamma}_{1-k\alpha/2}} \tag{E13}$$

Equation (E11) leads to the variance of the distribution:

$$\begin{aligned}\mathbb{V}\left[S_n\right] &= \mathbb{E}\left[S_n^2\right] - \left(\mathbb{E}\left[S_n\right]\right)^2 \\ &= (\lambda\pi)^{\alpha}\,\mathrm{e}^{\lambda\pi h^2}\left(\overline{A^2}\sum_{l=0}^{n-1}\frac{\left(-\lambda\pi h^2\right)^{n-l-1}}{l!\,(n-l-1)!}\,\tilde{\Gamma}_{1+l-\alpha}\right. \\ &\quad \left. - \mathrm{e}^{\lambda\pi h^2}\,\overline{A}^2\left(\sum_{l=0}^{n-1}\frac{\left(-\lambda\pi h^2\right)^{n-l-1}}{l!\,(n-l-1)!}\,\tilde{\Gamma}_{1+l-\alpha/2}\right)^2\right).\end{aligned} \tag{E14}$$

C. Exposure due to the n nearest BSs

The mean value of the total power density due to the n nearest BSs, $S_{[n]}$, is straightforward to obtain from (E8):

$$\begin{aligned}\mathbb{E}\left[S_{[n]}\right] &= \mathbb{E}\left[\sum_{i=1}^{n} S_i\right] = \sum_{i=1}^{n}\mathbb{E}\left[S_i\right] \\ &= \overline{A}\,(\lambda\pi)^{\alpha/2}\,\mathrm{e}^{\lambda\pi h^2}\sum_{i=1}^{n}\sum_{l=0}^{i-1}\frac{\left(-\lambda\pi h^2\right)^{i-l-1}}{l!\,(i-l-1)!}\,\tilde{\Gamma}_{1+l-\alpha/2},\end{aligned} \tag{E15}$$

where we used the assumption of uncorrelated BSs. The relative error made by truncating the network to the n nearest BSs is shown in Fig. F2. By taking only the closest BS, as often done in exposure studies, an error of 40% is committed. To have a relative error lower than 10%, it is necessary to take into account the 14 nearest BSs. The whole-network reference $\mathbb{E}\left[S_{WN}\right]$ will be derived in the following derivations (E29).

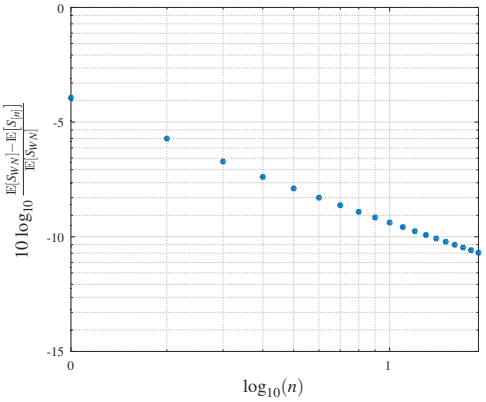

Fig. F2. Relative error between $\mathbb{E}\left[S_{[n]}\right]$ (E15) and $\mathbb{E}\left[S_{WN}\right]$ (E29). $\lambda = 13\,\text{BS/km}^2$, $\alpha = 2.90$, $h = 44\,\text{m}$, EIRP = 68.49 dBm.

Similarly, the k^{th} moment about zero of the resulting power density from the n nearest BSs is given by:

$$\begin{aligned}\mathbb{E}\left[S_{[n]}^k\right] &= \mathbb{E}\left[\left(\sum_{i=1}^{n} S(r_i)\right)^k\right] \\ &= \sum_{k_1+k_2+\ldots+k_n=k}\binom{k}{k_1,k_2,\cdots,k_n}\mathbb{E}\left[S_1^{k_1}S_2^{k_2}\cdots S_n^{k_n}\right] \\ &= \sum_{|\vec{k}|=k}\binom{k}{\vec{k}}\mathbb{E}\left[\prod_{i=1}^{n}S_i^{k_i}\right]\end{aligned} \tag{E16}$$

using the multinomial theorem [17], where

$$\binom{n}{k_1,k_2,k_3,\ldots,k_m} = \binom{n}{\vec{k}} = \frac{n!}{k_1!k_2!k_3!\cdots k_m!} = \frac{n!}{\prod_{i=1}^{m}k_i!} \tag{E17}$$

is a multinomial coefficient, generalization of the binomial coefficients. The quantity

$$\mathbb{E}\left[S_1^{m_1}S_2^{m_2}S_3^{m_3}\cdots S_n^{m_n}\right] \tag{E18}$$

appears in (E16). Its calculation is made in appendix A and leads to

$$\mathbb{E}\left[S_{[n]}^k\right] = \overline{A^k}\,(\lambda\pi)^{k\alpha/2}\,\mathrm{e}^{\lambda\pi h^2} \sum_{|\vec{k}|=k} \binom{k}{\vec{k}} \sum_{p=1}^{n-1} (-1)^{p-1} \left(\prod_{j=p+1}^{n-1} \frac{1}{\tau_{(p+1)}^{(j)}}\right) \times \left(\prod_{l=1}^{p} \frac{1}{\tau_{(l)}^{(p)}}\right) \left[\tilde{\Gamma}_{\tau_{(1)}^{(n)}} - \left(\lambda\pi h^2\right)^{\tau_{(1)}^{(p)}} \tilde{\Gamma}_{\tau_{(p+1)}^{(n)}}\right] \tag{E19}$$

where we use the following notations:

$$\tau_i = 1 - m_i\,\frac{\alpha}{2} \tag{E20a}$$

$$\tau_{(a)}^{(b)} = \begin{cases} \sum_{i=a}^{b} \tau_i & \text{if } a \le b \\ \tau_{(a)}^{(b)} = 0 & \text{if } a > b \end{cases} \tag{E20b}$$

Note that the case $k = 1$ corresponds to (E15). Again, the variance of the distribution can be deduced from (E19).

D. Whole network

Well-known mathematical results of signal-plus-interference-to-noise ratio and power coverage studies [18], [19], [20] can be adopted to study exposure. Still considering a PPP $\Phi \in \mathbb{R}^2$, the Laplace transform of (E3) can be calculated similarly to what is done in [21], chapter 1:

$$\begin{aligned}
\mathcal{L}_{S_{WN}}(s) &= \mathbb{E}\left[\mathrm{e}^{-s\,S_{WN}}\right] = \mathbb{E}_{\Phi,A}\left[\exp\left(-s\sum_{i\in\Phi}\frac{A}{\left(r_i^2+h^2\right)^{\alpha/2}}\right)\right] \\
&= \mathbb{E}_{\Phi,A}\left[\prod_{i\in\Phi}\exp\left(-s\,\frac{A}{\left(r_i^2+h^2\right)^{\alpha/2}}\right)\right] \\
&= \mathbb{E}_{\Phi}\left[\prod_{i\in\Phi}\mathbb{E}_A\left[\exp\left(-s\,\frac{A}{\left(r_i^2+h^2\right)^{\alpha/2}}\right)\right]\right] \\
&\overset{(a)}{=} \exp\left(2\pi\lambda\int_0^\infty \mathbb{E}_A\left[\exp\left(-s\,\frac{A}{\left(r^2+h^2\right)^{\alpha/2}}\right)-1\right] r\mathrm{d}r\right) \\
&\overset{(b)}{=} \exp\left(\frac{2\pi\lambda}{\alpha}\int_{h^\alpha}^\infty \mathbb{E}_A\left[\exp\left(-s\,\frac{A}{x}\right)-1\right] x^{2/\alpha-1}\mathrm{d}x\right) \\
&= \exp\left(\frac{2\pi\lambda}{\alpha}\int_{h^\alpha}^\infty \left(\mathbb{E}_A\left[\exp\left(-s\,\frac{A}{x}\right)\right]-1\right) x^{2/\alpha-1}\mathrm{d}x\right)
\end{aligned} \tag{E21}$$

(a) is the probability generating functional [22] and (b) is obtained using the change of variable $\left(r^2+h^2\right)^{\alpha/2} \to x$. $\mathbb{E}_A\left[\exp\left(-s\,\frac{A}{x}\right)\right]$ corresponds to the Laplace transform of A/x. Equation (E21) can therefore be calculated if the distribution of A is known.

If A is deterministic, $\mathbb{E}_A\left[\exp\left(-s\,\frac{A}{x}\right)\right] = \exp\left(-s\,\frac{A}{x}\right)$. Therefore

$$\begin{aligned}
\mathcal{L}_{S_{WN}}^{\text{determ.}}(s) &= \exp\left(\frac{2\pi\lambda}{\alpha}\int_{h^\alpha}^\infty\left(\exp\left(-s\,\frac{A}{x}\right)-1\right)x^{2/\alpha-1}\mathrm{d}x\right) \\
&= \exp\left(\pi\lambda\,h^2\left[1-{}_1F_1\left(-2/\alpha;1-2/\alpha;\frac{-s\,A}{h^\alpha}\right)\right]\right)
\end{aligned} \tag{E22}$$

using the relationship [23]

$$\int_a^\infty \left(\exp\left(\frac{b}{z}\right)-1\right) z^{v-1}\mathrm{d}z = \frac{1}{v}\,a^v\,\left[1-{}_1F_1\left(-v;1-v;{}^b/_a\right)\right]. \tag{E23}$$

where ${}_1F_1(a;b;z)$ is the Kummer confluent hypergeometric function. [20] gives an excellent approximation for (E22), which can be used for numerical calculations:

$$\mathcal{L}_{S_{WN}}(s) \approx \begin{cases} \exp\left(\pi\lambda\,h^2\sum_{j=1}^{\infty}\frac{2\,(-sA)^j}{h^{\alpha j}\,j!\,(j\,\alpha-2)}\right), & \left|\frac{s\,A}{h^\alpha}\right| \le c \\ \exp\left(\pi\lambda\,h^2\left(\frac{-(s\,A)^{2/\alpha}}{h^2}\,\Gamma\left(1-\frac{2}{\alpha}\right)+1\right)\right), & \left|\frac{s\,A}{h^\alpha}\right| > c \end{cases} \tag{E24}$$

No analytical solution exists for c, the intersection point of the two parts of (E24). Moreover, several solutions often exist. For numerical calculations, it is preferable to take the largest solution in absolute value.

For a Rayleigh fading, we let $A = p\,B$ where $p = \frac{\text{EIRP}}{4\pi}$ and $B \sim \text{Exp}(1)$, an exponential random variable with unit rate, so that $\mathbb{E}[B] = 1$. Starting again from (E21), the following result holds:

$$\mathbb{E}_A\left[\exp\left(-s\,\frac{A}{x}\right)\right] = \frac{1}{1+\frac{p\,s}{x}} \tag{E25}$$

$$\begin{aligned}
\mathcal{L}_{S_{WN}}^{Rayleigh}(s) &= \exp\left(\frac{2\pi\lambda}{\alpha}\int_{h^\alpha}^\infty\left(\frac{1}{1+\frac{s\,p}{x}}-1\right)x^{2/\alpha-1}\mathrm{d}x\right) \\
&= \exp\left(\frac{-2\pi\lambda}{\alpha}\int_{h^\alpha}^\infty\frac{1}{(s\,p)^{-1}\,x+1}\,x^{2/\alpha-1}\mathrm{d}x\right) \\
&\overset{(a)}{=} \exp\left(\frac{-2\pi\lambda}{\alpha}\,s\,p\,h^{2-\alpha}\int_0^\infty\frac{1}{y+s\,p\,h^{-\alpha}+1}\,(y+1)^{2/\alpha-1}\,\mathrm{d}y\right) \\
&\overset{(b)}{=} \exp\left(\frac{-2\pi\lambda}{\alpha-2}\,s\,p\,h^{2-\alpha}\,{}_2F_1\left(1,1-2/\alpha;2-2/\alpha;\frac{-s\,p}{h^\alpha}\right)\right),
\end{aligned} \tag{E26}$$

using (a) the change of variable $x\,h^{-\alpha}-1 \to y$ and (b) the relationship [24]

$$\int_0^\infty t^{-b+c-1}\,(t+1)^{a-c}\,(t-z+1)^{-a}\,\mathrm{d}t = \frac{\Gamma(b)\,\Gamma(c-b)}{\Gamma(c)}\,{}_2F_1(a,b;c;z) \tag{E27}$$

where ${}_2F_1(a,b;c;z)$ is the Gauss confluent hypergeometric function. The CDF of S_{WN} is then numerically obtained by applying the inversion theorem [25]:

$$F(x) = \frac{1}{2} - \frac{1}{\pi}\int_0^\infty \frac{\Im\left[\mathrm{e}^{-itx}\,\mathcal{L}_S(-it)\right]}{t}\,dt. \tag{E28}$$

Consequently, using $E = \sqrt{Z_0 \cdot S}$ for the x-axis, we finally obtain the CDF of E. A comparison between CDFs with and without Rayleigh fading with rate 1 is shown in Fig. F3. As expected, the no-fading case overestimates the exposure but the difference with the unit-rate Rayleigh-fading case is not big, as suggests the Kolmogorov-Smirnov distance of 0.07 between the CDFs. In the following, we only work under a no-fading hypothesis, which is moreover faster to compute numerically thanks to the approximation (E24). The CDF, for different values of λ, α and h, are respectively shown in Fig. F4, Fig. F5 and Fig. F6 which makes it possible to observe the impact of these parameters on the shape of the CDF.

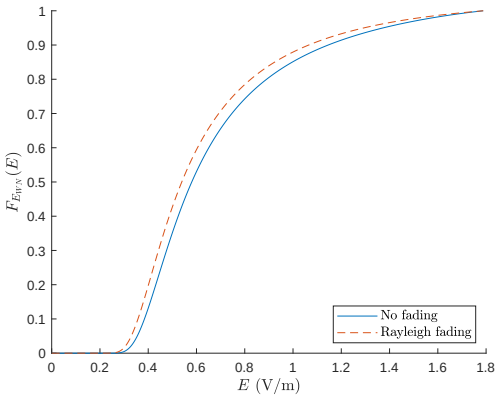

Fig. F3. CDF $F_{E_{WN}}$ with a Rayleigh fading and without fading. $\lambda = 13\,\text{BS/km}^2$, $\alpha = 2.90$, $h = 44\,\text{m}$, EIRP = 68.49 dBm.

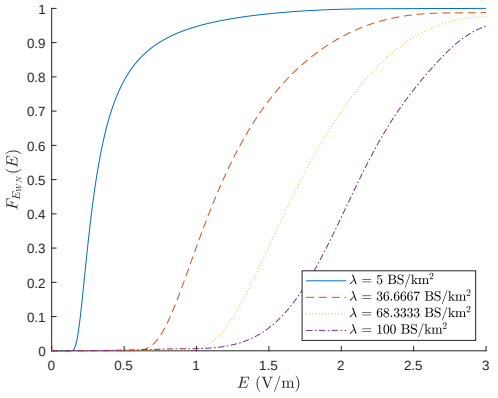

Fig. F4. CDF $F_{E_{WN}}$ for several values of λ. $\alpha = 2.90$, $h = 44\,\text{m}$, EIRP = 68.49 dBm.

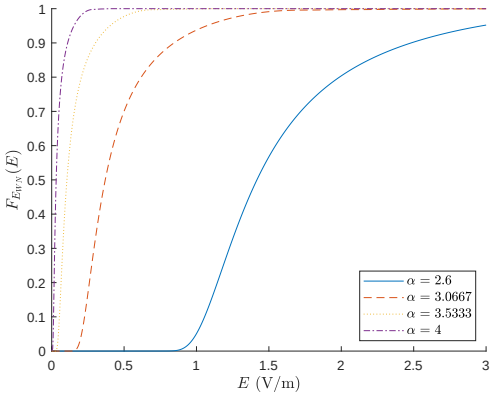

Fig. F5. CDF $F_{E_{WN}}$ for several values of α. $\lambda = 13\,\text{BS/km}^2$, 44 m, EIRP = 68.49 dBm.

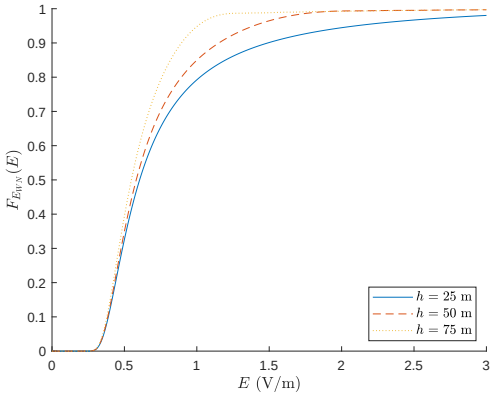

Fig. F6. CDF $F_{E_{WN}}$ for several values of h. $\lambda = 13\,\text{BS/km}^2$, $\alpha = 2.90$, EIRP = 68.49 dBm.

Clearly, the path loss exponent has the greatest impact on exposure.

The mean is given by

$$\begin{aligned}
\mathbb{E}\left[S_{WN}\right] &= \mathbb{E}\left[\sum_{i\in\Phi} S(r_i)\right] \\
&= \mathbb{E}_{\Phi,A}\left[\sum_{i\in\Phi} \frac{A}{\left(r_i^2+h^2\right)^{\alpha/2}}\right] \\
&= \lambda\,\overline{A}\int_0^{2\pi} \mathrm{d}\theta \int_0^{\infty} \frac{1}{\left(r^2+h^2\right)^{\alpha/2}}\, r\,\mathrm{d}r \\
&= 2\pi\lambda\,\overline{A}\int_h^{\infty} \frac{1}{t^{\alpha}}\, t\,\mathrm{d}t \\
&= \frac{2\pi\lambda\,\overline{A}}{2-\alpha}\left[t^{2-\alpha}\right]_h^{\infty} \\
&= \frac{2\pi\lambda\,\overline{A}}{\alpha-2}\,\frac{1}{h^{\alpha-2}}
\end{aligned} \tag{E29}$$

where we used Campbell's formula [26] and where we implicitly assumed that $\alpha > 2$. Equation (E29) clearly shows the relative impact of the BS density, the path loss exponent and the BS height on the mean exposure. Similarly, the variance of the distribution is

$$\begin{aligned}
\mathbb{V}\left[S_{WN}\right] &= \mathbb{E}\left[\sum_{i\in\Phi} S^2(r_i)\right] \\
&= \mathbb{E}_A\left[A^2\right]\cdot\mathbb{E}_{\Phi}\left[\sum_{i\in\Phi} \frac{1}{\left(r_i^2+h^2\right)^{\alpha}}\right] \\
&= 2\pi\lambda\,\overline{A^2}\int_0^{\infty} \frac{1}{\left(r^2+h^2\right)^{\alpha}} r\,\mathrm{d}r \\
&= 2\pi\lambda\,\overline{A^2}\int_h^{\infty} \frac{1}{t^{2\alpha}}\, t\,\mathrm{d}t \\
&= \frac{2\pi\lambda\,\overline{A^2}}{2-\alpha}\left[t^{2-\alpha}\right]_h^{\infty} \\
&= \frac{2\pi\lambda\,\overline{A^2}}{2\alpha-2}\,\frac{1}{h^{2\alpha-2}}
\end{aligned} \tag{E30}$$

with $\overline{A^2} = \mathbb{E}_A\left[A^2\right]$. Equations (E29) and (E30) are valid no matter the fading distribution chosen for A.

3. EXPERIMENTAL RESULTS

Using the open access databases of BS locations available in Belgium [27], the BS density for all network providers together was calculated over the Brussels-Capital Region in Belgium. Since nearly all BSs were found to contain antennas for all cellular services and since the antenna density by service is not always available, we assumed that the density of BSs is the same no matter the service: $\lambda = 13\,\mathrm{BS/km^2}$.

Statistical distributions for the power density were experimentally obtained by drive-tests in a zone of $4.37\,\mathrm{km}^2$ that spans two municipalities (Ixelles and Etterbeek) of Brussels. The comprehensive experimental set-up is described in [2]. A spectrum analyzer was mounted on a moving car, taking calibrated measurements in the UMTS 2100 and LTE 2600 frequency bands with a resolution bandwith of 3 MHz. A GPS was used to tag the measurements with position. Measurements were averaged over squared local areas of $2\,\mathrm{m} \times 2\,\mathrm{m}$. This size was heuristically chosen, small enough to keep a relevant spatial sampling, but large enough to smooth out fading. Measurements were obtained for around 16 000 $4\,\mathrm{m}^2$-squares. We focused on the UMTS 2100 and LTE 2600 frequency bands:

$$S_{UMTS2100} = \sum_{f=2\,110.3\,\mathrm{MHz}}^{2\,140.1\,\mathrm{MHz}} S_f + \sum_{f=2\,154.9\,\mathrm{MHz}}^{2\,169.7\,\mathrm{MHz}} S_f \quad \text{(E31)}$$

$$S_{LTE2600} = \sum_{f=2\,620\,\mathrm{MHz}}^{2\,640\,\mathrm{MHz}} S_f + \sum_{f=2\,655\,\mathrm{MHz}}^{2\,690\,\mathrm{MHz}} S_f \quad \text{(E32)}$$

where S_f is the power density measured at frequency f.

Parameters of the model (E1)-(E3) under the no-fading hypothesis have been fitted by minimizing

$$\begin{aligned} K(\theta) = &\left(\frac{Q_{05}(\theta)}{Q_{05,exp}} - 1\right)^2 + \left(\frac{Q_{10}(\theta)}{Q_{10,exp}} - 1\right)^2 + \left(\frac{Q_{25}(\theta)}{Q_{25,exp}} - 1\right)^2 \\ &+ \left(\frac{Q_{50}(\theta)}{Q_{50,exp}} - 1\right)^2 + \left(\frac{Q_{75}(\theta)}{Q_{75,exp}} - 1\right)^2 + \left(\frac{Q_{90}(\theta)}{Q_{90,exp}} - 1\right)^2 \\ &+ \left(\frac{Q_{95}(\theta)}{Q_{95,exp}} - 1\right)^2 + \left(\frac{\mu(\theta)}{\mu_{exp}} - 1\right)^2 \end{aligned} \quad \text{(E33)}$$

where $\theta = (h, \alpha, \mathrm{EIRP})$ is the 3-tuple of parameters. Q_x is the x%-quantile and μ the mean of the distribution of S_{WN} using θ. The notation "x_{exp}" refers to statistics obtained from the experimental distribution. The minimization of $K(\theta)$ is an exhaustive search onto a regular grid $\mathcal{G} = \mathcal{I}_h \times \mathcal{I}_\alpha \times \mathcal{I}_{EIRP}$ with $\mathcal{I}_h = [10; 60]$m with a step of 1 m, $\mathcal{I}_\alpha = [2; 5]$ with a step of 0.05 and $\mathcal{I}_{EIRP} = [56.0; 81.0]$dBm with a step of 0.01 dBm.

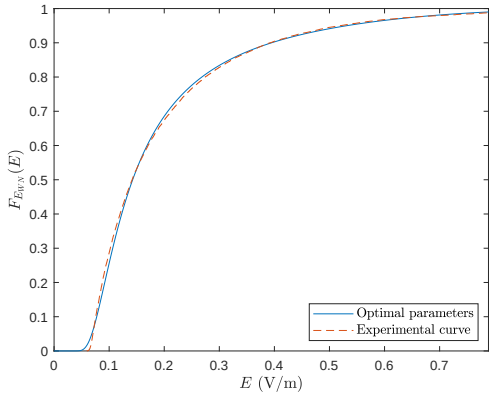

Fig. F7. CDF of E for the network made of BSs from all network providers in Brussels for the UMTS 2100 band.

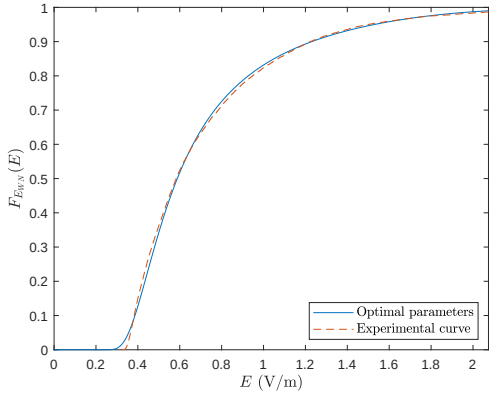

Fig. F8. CDF of E for the network made of BSs from all network providers in Brussels for the LTE 2600 band.

Table T1. *Parameters of the statistical distributions of the power density for the UMTS 2100 and LTE 2600 frequency bands, in the Brussels-Capital Region (Ixelles and Etterbeek). Exp: experimental results. SG: CDF obtained by a numeric Gil-Pelaez inversion. Q_x's are the quantiles, μ the mean.*

Frequency band	UMTS 2100		LTE 2600	
	Exp	SG	Exp	SG
h (m)	40		44	
α	3.35		2.90	
EIRP (dBm)	66.80		68.49	
Q_{05} (W/m^2)	$1.32 \cdot 10^{-5}$	$1.26 \cdot 10^{-5}$	$3.54 \cdot 10^{-4}$	$3.36 \cdot 10^{-4}$
Q_{10} (W/m^2)	$1.52 \cdot 10^{-5}$	$1.57 \cdot 10^{-5}$	$3.88 \cdot 10^{-4}$	$3.95 \cdot 10^{-4}$
Q_{25} (W/m^2)	$2.35 \cdot 10^{-5}$	$2.58 \cdot 10^{-5}$	$5.20 \cdot 10^{-4}$	$5.53 \cdot 10^{-4}$
Q_{50} (W/m^2)	$5.32 \cdot 10^{-5}$	$5.40 \cdot 10^{-5}$	$9.02 \cdot 10^{-4}$	$9.18 \cdot 10^{-4}$
Q_{75} (W/m^2)	$1.52 \cdot 10^{-4}$	$1.44 \cdot 10^{-4}$	$1.94 \cdot 10^{-3}$	$1.86 \cdot 10^{-3}$
Q_{90} (W/m^2)	$4.08 \cdot 10^{-4}$	$4.13 \cdot 10^{-4}$	$3.97 \cdot 10^{-3}$	$4.02 \cdot 10^{-3}$
Q_{95} (W/m^2)	$7.15 \cdot 10^{-4}$	$7.49 \cdot 10^{-4}$	$5.98 \cdot 10^{-3}$	$6.20 \cdot 10^{-3}$
μ (W/m^2)	$1.76 \cdot 10^{-4}$	$1.55 \cdot 10^{-4}$	$1.80 \cdot 10^{-3}$	$1.65 \cdot 10^{-3}$
KS distance	0.04		0.03	

Statistical parameters of the distributions are listed in table T1. The optimal set of parameters for the propagation model (E3) are also listed in this table.

As seen in Fig. F7 and Fig. F8, the SG CDFs well fit the experimental ones. The x-axis is expressed in terms of electric field strengths E instead of power densities using (E1). The gap between the curves for small values of E is due to background noise. To estimate goodness-of-fit, the two-sample Kolmogorov-Smirnov (KS) distance, based on cumulative distribution functions, is computed at the end of the table. Fitted values for h, α and EIRP are realistic on physical grounds.

Taking the distribution of the power density due to the nearest BS, S_1, leads to a mean power density of $9.85 \cdot 10^{-4}\,\mathrm{W/m^2}$ (computed from (E5)) instead of $1.65 \cdot 10^{-3}\,\mathrm{W/m^2}$ when considering all the BSs (from (E29)) for the LTE 2600 frequency band. Expressed in terms of the electric field strengths, these values respectively correspond to 0.61 V/m and 0.79 V/m. Similarly, for the LTE 2600 band, the median and the 95%-quantile of the electric field are respectively 0.36 V/m and 1.32 V/m for the nearest-BS approximation against 0.59 V/m and 1.53 V/m when the whole set of BSs is used.

4. CONCLUSION

In this paper, we introduced the use of stochastic geometry for exposure assessment. We showed some general mathematical expressions of the statistics of the power density, coming from a limited number of the network's BSs or from all BSs. In particular, we obtained a numerical CDF of the power density due to all BSs for a simple propagation model, when the BS pattern can be approached by a PPP. The CDF of the electric field was deduced from it, allowing to compute statistics and probabilities to reach electric field thresholds. We then applied this framework to experimental measurements realized in Brussels, Belgium. We showed that the model gives results very faithful to reality for the UMTS2100 and LTE2600 cellular services.

A. EXPECTED VALUE OF A PRODUCT OF POWERS OF POWER DENSITIES

We evaluate (E18),

$$\mathbb{E}\left[S_1^{m_1} S_2^{m_2} S_3^{m_3} \cdots S_n^{m_n}\right]. \tag{E34}$$

We define $M = \sum_{i=1}^{n} m_i$ and we use some properties of (E20a) and (E20b):

$$\tau_i = \tau_{(i)}^{(i)}, \tag{E35}$$

$$\tau_{(a)}^{(b)} + \tau_{(b+1)}^{(c)} = \tau_{(a)}^{(c)}. \tag{E36}$$

Moreover, we use, as previously, the change of variable $\lambda\pi\left(r_i^2 + h^2\right) \to t_i$ and the following properties involving the upper incomplete Gamma function:

Integration property

$$\begin{aligned}\int_l^\infty t^{b-1}\,\Gamma(z,t)\,\mathrm{d}t &\overset{(a)}{=} \left[\frac{t^b}{b}\,\Gamma(z,t)\right]_l^\infty + \frac{1}{b}\int_l^\infty t^{b-1+z}\,\mathrm{e}^{-t}\,\mathrm{d}t \\ &\overset{(b)}{=} \frac{1}{b}\left(\Gamma(b+z,l) - l^b\,\Gamma(z,l)\right),\end{aligned} \tag{E37}$$

using (a) an integration by parts and (b) the result $\lim_{t\to\infty} t^b\,\Gamma(z,t) = 0$.

Particular case $b = 1$

$$\int_l^\infty \Gamma(z,t)\,\mathrm{d}t = \Gamma(1+z,l) - l\,\Gamma(z,l). \tag{E38}$$

Recurrence formula

$$\begin{aligned}\Gamma(z+1,t) &= \int_t^\infty u^z\,\mathrm{e}^{-u}\,\mathrm{d}u \\ &= \left[-u^z\,\mathrm{e}^{-u}\right]_t^\infty + z\int_t^\infty u^{z-1}\,\mathrm{e}^{-u}\,\mathrm{d}u \\ &= t^z\,\mathrm{e}^{-t} + z\,\Gamma(z,t).\end{aligned} \tag{E39}$$

$$\begin{aligned}\mathbb{E}\left[S_1^{m_1} S_2^{m_2} \cdots S_n^{m_n}\right] &= \overline{A^M}\,(\lambda\pi)^{M\alpha/2}\,\mathrm{e}^{\lambda\pi h^2}\int_{\lambda\pi h^2}^\infty t_1^{-\alpha/2\,m_1} \\ &\times \underbrace{\int_{t_1}^\infty t_2^{-\alpha/2\,m_2}\cdots\int_{t_{n-1}}^\infty t_n^{-\alpha/2\,m_n}\,\mathrm{e}^{-t_n}\,\mathrm{d}t_n\cdots\mathrm{d}t_2}_{*}\,\mathrm{d}t_1\end{aligned} \tag{E40}$$

using the joint probability distribution for the n nearest BSs

$$\begin{aligned}&f(r_1, r_2, \cdots, r_n)\,\mathrm{d}r_1\,\mathrm{d}r_2\cdots\mathrm{d}r_n \\ &\qquad = (2\lambda\pi)^n\,\mathrm{e}^{-\lambda\pi r_n^2}\,r_1\,r_2\cdots r_n\,\mathrm{d}r_1\,\mathrm{d}r_2\cdots\mathrm{d}r_n.\end{aligned} \tag{E41}$$

Let us extract the term underbraced by a star for convenience:

$$
\begin{aligned}
&\int_{t_1}^{\infty} t_2^{-\alpha/2\, m_2} \cdots \int_{t_{n-1}}^{\infty} t_n^{-\alpha/2\, m_n}\, \mathrm{e}^{-t_n}\, \mathrm{d}t_n \cdots \mathrm{d}t_2 \\
&= \int_{t_1}^{\infty} t_2^{-\alpha/2\, m_2} \cdots \int_{t_{n-2}}^{\infty} \Gamma\left(\overbrace{1-\alpha/2\, m_n}^{\tau_n}, t_{n-1}\right) \\
&\quad \times t_{n-1}^{\alpha/2\, m_{n-1}}\, \mathrm{d}t_{n-1} \cdots \mathrm{d}t_2 \\
&= \int_{t_1}^{\infty} t_2^{\tau_2-1} \cdots \int_{t_{n-3}}^{\infty} \frac{1}{\tau_{n-1}} \left[\Gamma\left(\tau_{(n-1)}^{(n)}, t_{n-2}\right)\right. \\
&\quad \left. -t_{n-2}^{\tau_n-1}\, \Gamma\left(\tau_n, t_{n-2}\right)\right] t_{n-2}^{\tau_{n-2}-1}\, \mathrm{d}t_{n-2} \cdots \mathrm{d}t_2 \\
&= \int_{t_1}^{\infty} t_2^{\tau_2-1} \cdots \int_{t_{n-4}}^{\infty} \left[\frac{1}{\tau_{n-1}\, \tau_{n-2}} \Gamma\left(\tau_{(n-2)}^{(n)}, t_{n-3}\right)\right. \\
&\quad - \frac{t_{n-3}^{\tau_{n-2}}}{\tau_{n-1}\, \tau_{n-2}} \Gamma\left(\tau_{(n-1)}^{(n)}, t_{n-3}\right) - \frac{1}{\tau_{n-1}\, \tau_{(n-2)}^{(n-1)}} \Gamma\left(\tau_{(n-2)}^{(n)}, t_{n-3}\right) \\
&\quad \left. + \frac{t_{n-3}^{\tau_{(n-2)}^{(n-1)}}}{\tau_{n-1}\, \tau_{(n-2)}^{(n-1)}} \Gamma\left(\tau_n, t_{n-3}\right)\right] t_{n-3}^{\tau_{n-3}-1}\, \mathrm{d}t_{n-3} \cdots \mathrm{d}t_2 \\
&= \int_{t_1}^{\infty} t_2^{\tau_2-1} \cdots \int_{t_{n-4}}^{\infty} \left[\frac{1}{\tau_{(n-2)}^{(n-1)}\, \tau_{(n-2)}^{(n-2)}} \Gamma\left(\tau_{(n-2)}^{(n)}, t_{n-3}\right)\right. \\
&\quad - \frac{t_{n-3}^{\tau_{(n-2)}^{(n-2)}}}{\tau_{(n-1)}^{(n-1)}\, \tau_{(n-2)}^{(n-2)}} \Gamma\left(\tau_{(n-1)}^{(n)}, t_{n-3}\right) \\
&\quad \left. + \frac{t_{n-3}^{\tau_{(n-2)}^{(n-1)}}}{\tau_{(n-1)}^{(n-1)}\, \tau_{(n-2)}^{(n-1)}} \Gamma\left(\tau_{(n)}^{(n)}, t_{n-3}\right)\right] t_{n-3}^{\tau_{n-3}-1}\, \mathrm{d}t_{n-3} \cdots \mathrm{d}t_2 \\
&= \ldots \\
&= \sum_{p=1}^{n-1} (-1)^{p-1} \left(\prod_{j=p+1}^{n-1} \frac{1}{\tau_{(p+1)}^{(j)}}\right) \left(\prod_{l=2}^{p} \frac{1}{\tau_{(l)}^{(p)}}\right) \Gamma\left(\tau_{(p+1)}^{(n)}, t_1\right)\, t_1^{\tau_{(2)}^{(p)}}.
\end{aligned}
\tag{E42}
$$

Using (E36) and replacing (E42) in (E40), we can calculate (E18):

$$
\begin{aligned}
\mathbb{E}\left[S_1^{m_1} S_2^{m_2} \cdots S_n^{m_n}\right] &= \overline{A^M}\, (\lambda\pi)^{M\alpha/2}\, \mathrm{e}^{\lambda\pi h^2} \sum_{p=1}^{n-1} (-1)^{p-1} \\
&\times \left(\prod_{j=p+1}^{n-1} \frac{1}{\tau_{(p+1)}^{(j)}}\right) \left(\prod_{l=1}^{p} \frac{1}{\tau_{(l)}^{(p)}}\right) \left[\tilde{\Gamma}_{\tau_{(1)}^{(n)}} - \left(\lambda\pi h^2\right)^{\tau_{(1)}^{(p)}} \tilde{\Gamma}_{\tau_{(p+1)}^{(n)}}\right].
\end{aligned}
\tag{E43}
$$

REFERENCES

1. S. Aerts, L. Verloock, M. Van Den Bossche, D. Colombi, L. Martens, C. Törnevik, and W. Joseph, "In-situ Measurement Methodology for the Assessment of 5G NR Massive MIMO Base Station Exposure at Sub-6 GHz Frequencies," IEEE Access **7**, 184658–184667 (2019).
2. T. Lemaire, J. Wiart, and P. De Doncker, "Variographic analysis of public exposure to electromagnetic radiation due to cellular base stations: Variographic Analysis of BTS EMF Exposure," Bioelectromagnetics **37** (2016).
3. S. Aerts, J. Wiart, L. Martens, and W. Joseph, "Assessment of long-term spatio-temporal radiofrequency electromagnetic field exposure," Environ. Res. **161**, 136 – 143 (2018).
4. S. Shikhantsov, A. Thielens, G. Vermeeren, P. Demeester, L. Martens, G. Torfs, and W. Joseph, "Massive MIMO Propagation Modeling With User-Induced Coupling Effects Using Ray-Tracing and FDTD," IEEE J. on Sel. Areas Commun. **38**, 1955–1963 (2020).
5. F. Baccelli and B. Blaszczyszyn, "Stochastic Geometry and Wireless Networks: Volume I Theory," Foundations Trends Netw. **3**, 249–449 (2009).
6. A. Al-Hourani, R. J. Evans, S. Kandeepan, B. Moran, and H. Eltom, "Stochastic Geometry Methods for Modeling Automotive Radar Interference," IEEE Transactions on Intell. Transp. Syst. **19**, 333–344 (2018).
7. C. E. O'Lone, H. S. Dhillon, and R. M. Buehrer, "A Statistical Characterization of Localization Performance in Wireless Networks," IEEE Transactions on Wirel. Commun. **17**, 5841–5856 (2018).
8. M. Filo, C. H. Foh, S. Vahid, and R. Tafazolli, "Stochastic Geometry Analysis of Ultra-Dense Networks: Impact of Antenna Height and Performance Limits," (2017).
9. R. Mathar and J. Mattfeldt, "On the distribution of cumulated interference power in Rayleigh fading channels," Wirel. Networks **1**, 31–36 (1995).
10. J. Andrews, A. Gupta, and H. Dhillon, "A Primer on Cellular Network Analysis Using Stochastic Geometry," (2016).
11. M. A. Hajj, S. Wang, P. De Doncker, C. Oestges, and J. Wiart, "A Statistical Estimation of 5G Massive MIMO's Exposure using Stochastic Geometry," in *2020 XXXIIIrd General Assembly and Scientific Symposium of the International Union of Radio Science*, (2020), pp. 1–3.
12. ICNIRP, "ICNIRP Guidelines for Limiting Exposure to Electromagnetic Fields (100 kHz to 300 GHz)," Heal. Phys. **118**, 483–524 (2020).
13. I. T. Union, "Measurement of radio frequency electromagnetic fields to determine compliance with human exposure limits when a base station is put into service," (2019). 07/2019. FEMU ID: 39880; EMF-Portal URL: https://www.emf-portal.org/en/article/39880.
14. J. S. Gomez, A. Vasseur, A. Vergne, P. Martins, L. Decreusefond, and W. Chen, "A Case Study on Regularity in Cellular Network Deployment," IEEE Wirel. Commun. Lett. **4**, 421–424 (2015).
15. H. Thompson, "Distribution of distance to nth neighbour in a population of randomly distributed individuals," Ecology. **37** (1956).
16. M. Abramowitz and I. A. Stegun, *Handbook of Mathematical Functions with Formulas, Graphs, and Mathematical Tables* (Dover, New York, 1964), chap. Gamma Function and Related Function, p. 263, 9th Dover printing, 10th GPO printing ed.

17. K. K. Kataria, "A Probabilistic Proof of the Multinomial Theorem," The Am. Math. Mon. **123**, 94–96 (2016).
18. W. Bi, L. Xiao, X. Su, and S. Zhou, "Fractional full duplex cellular network: a stochastic geometry approach," Sci. China Inf. Sci. **61**, 1–15 (2016).
19. F. Baccelli and B. Błaszczyszyn, "Stochastic Geometry and Wireless Networks: Volume II Applications," Foundations Trends Netw. **4**, 1–312 (2010).
20. A. Aravanis, T. Tu, O. Muñoz, A. Pascual-Iserte, and M. Di Renzo, "A tractable closed form approximation of the ergodic rate in Poisson cellular networks," EURASIP J. on Wirel. Commun. Netw. **12** (2019).
21. L. T. Tu, "New Analytical Methods for the Analysis and Optimization of Energy-Efficient Cellular Networks by Using Stochastic Geometry," Theses, Université Paris-Saclay (2018).
22. M. Haenggi, *Stochastic Geometry for Wireless Networks* (Cambridge University Press, 2012).
23. M. Renzo and W. Lu., "System-level analysis/optimization of cellular networks with simultaneous wireless information and power transfer: Stochastic geometry modeling," IEEE Transactions on Veh. Technol. **66**, 2251–2275 (2017).
24. S. Saran, "Hypergeometric functions of three variables," Ganita. **5**, 77–91 (1954).
25. J. Gil-Pelaez, "Note on the inversion theorem," Biometrika. **38**, 481–482 (1951).
26. J. F. C. Kingman, *Poisson processes* (The Clarendon Press Oxford University Press, New York, 1993), vol. 3 of *Oxford Studies in Probability*, chap. Sums over Poisson processes, pp. 28–29. Oxford Science Publications.
27. IBPT/BIPT (2019). [Online]. Available: https://www.ibpt.be/en/operators/radio/antennas-site-sharing/antennas-cartography.